BLIND DT-CWT DOMAIN ADDITIVE SPREAD-SPECTRUM WATERMARK DETECTION

Roland Kwitt and Peter Meerwald and Andreas Uhl

Department of Computer Sciences,
University of Salzburg, Austria
{rkwitt, pmeerw, uhl}@cosy.sbg.ac.at

ABSTRACT

In this paper, we adapt two blind detector structures for additive spread-spectrum image watermarking to the host signal characteristics of the Dual-Tree Complex Wavelet Transform (DT-CWT) domain coefficients. The research is motivated by the superior perceptual characteristics of the DT-CWT and its active use in watermarking. To improve the numerous existing watermarking schemes in which the host signal is modeled by a Gaussian distribution, we show that the Generalized Gaussian nature of Dual-Tree detail subband statistics can be exploited for better detector performance. We found that the Rao detector is more practical than the likelihood-ratio test for our detection problem. We experimentally investigate the robustness of the proposed detectors under JPEG and JPEG2000 attacks and assess the perceptual quality of the watermarked images. The results demonstrate that our alterations allow significantly better blind watermark detection performance in the DT-CWT domain than the widely used linear-correlation detector.

Index Terms— watermarking, dual-tree complex wavelet transform, detection

1. INTRODUCTION

Watermarking has been proposed as a technology to ensure copyright protection by embedding an imperceptible, yet detectable signal in digital multimedia content such as images or video. Transform domains such as the DCT or DWT facilitate modeling human perception and permit selection of signal components which can be watermarked in a robust but unobtrusive way.

Loo et al. [1] first proposed to use Kingsbury's dual-tree complex wavelet transform (DT-CWT) [2] for blind watermarking. The DT-CWT is a complex wavelet transform variant which is only four-times redundant in 2-D and offers approximate shift invariance together with the property of directional selectivity. Thus, it remedies two commonly-known shortcomings of the classic, maximally decimated DWT. Furthermore, it can be implemented very efficiently on the basis of four parallel 2-D DWTs.

Supported by Austrian Science Fund project FWF-P19159-N13.

For these reasons, the DT-CWT domain has become a very popular choice for watermark embedding recently [1, 3, 4, 5, 6, 7, 8]. However, for blind watermarking detection, i.e. when detection is performed without reference to the unwatermarked host signal, the host interferes with the watermark signal. Hence informed embedding/coding techniques at the embedder side (e.g. ISS [9]) and, at the detector side, accurate modelling of the host signal is crucial for the overall performance of a blind watermarking scheme. In this paper, we focus on improving the detector part.

In section 2 we argue that the real and imaginary parts of DT-CWT subband coefficients can be accurately modeled by a Generalized Gaussian distribution (GGD). After reviewing the literature on complex wavelet domain watermarking in section 3, we adopt and compare the applicability of two blind spread-spectrum watermark detectors in section 4 which exploits the DT-CWT domain subband statistics. We experimentally compare the detection performance of the proposed schemes also under JPEG and JPEG2000 attacks and assess the perceptual quality of DT-CWT embedding in section 5. Section 6 offers concluding remarks.

2. DT-CWT SUBBAND STATISTICS

In order to obtain a good signal detector in noise, i.e. the host signal for blind watermarking in the absence of attacks, we have to find a reasonable noise model first. By employing a J-scale 2-D DT-CWT we obtain six complex subbands per decomposition level, oriented along approximately $\pm 15°, \pm 45°, \pm 75°$. To visualize the directional selectivity, Figure 1 shows the magnitude of six complex detail subbands at level two of the decomposed Bridge image (see Figure 4(d)). The subbands will be denoted by $\mathbf{D}_{sk} = \{d_{sk,ij}\}_{1 \leq i,j \leq n_s}$, where the decomposition level is given by $s, 1 \leq s \leq J$ and $k, 1 \leq k \leq 6$ denotes the orientation. Further, we recognize that $d_{sk,ij} \in \mathbb{C}$. The number of coefficients per subband on level s is given by n_s^2 (for square subbands). The matrix $\mathbf{D}_{sk}$ can also be written in vector notation as $\mathbf{d}_{sk} = [d_{sk,11}, d_{sk,21}, \dots, d_{sk,n_s 1}, \dots, d_{sk,1 n_s}, \dots, d_{sk,n_s n_s}]$, where we have simply rearranged the column vectors into one big row vector. We propose that the marginal distri-

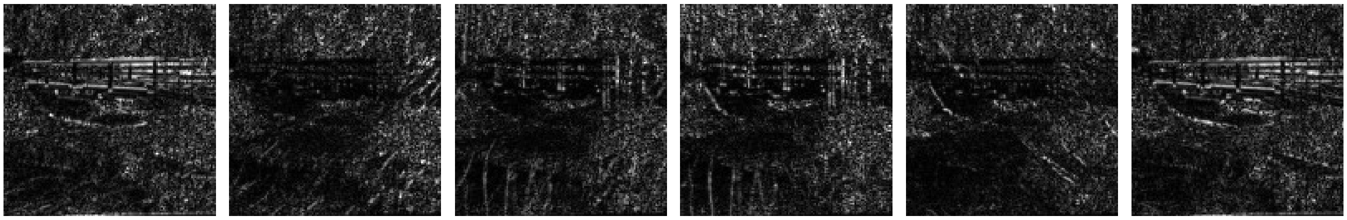

(a) $\hat{\beta} = 0.94$ (b) $\hat{\beta} = 0.81$ (c) $\hat{\beta} = 0.81$ (d) $\hat{\beta} = 0.82$ (e) $\hat{\beta} = 0.81$ (f) $\hat{\beta} = 0.93$

Fig. 1. Complex coefficient magnitudes of the 2^{nd} level detail subbands with the MLEs of the GGD's shape parameter β fitted to the marginal distributions of concatenated real and imaginary parts.

	Orientation					
Scale	$15°$	$45°$	$75°$	$-75°$	$-45°$	$-15°$
1	6, 5	4, 3	6, 6	6, 5	4, 4	6, 6
2	4, 5	2, 4	4, 4	3, 3	3, 3	5, 4
3	2, 0	0, 0	1, 2	1, 2	1, 0	1, 1

Table 1. Rejected null-hypothesis for the χ^2 GoF outcomes at 1% significance (6 images).

	Orientation					
Scale	$15°$	$45°$	$75°$	$-75°$	$-45°$	$-15°$
1	6	6	6	6	6	6
2	0	0	0	1	0	0
3	1	0	0	1	0	0

Table 2. Rejections for the two-sample KS tests at 1% significance (6 images).

butions of the real and imaginary parts of complex wavelet coefficients of scales $s \geq 2$ can be modeled by two-parameter GGDs. The probability density function (PDF) of a GGD is given by [10]

$$p(x; \alpha, \beta) = \frac{\beta}{2\alpha\Gamma(1/\beta)} \exp\left\{-\left|\frac{x}{\alpha}\right|^{\beta}\right\}, \quad -\infty < x < \infty \tag{1}$$

with parameters $\alpha > 0$ (scale) and $\beta > 0$ (shape). In case of $\beta = 1$ the PDF reduces to the Laplace distribution, in case of $\beta = 2$ we obtain the Gaussian distribution. To verify the suitability of the proposed distributional model, we employ a Chi-Square Goodness-of-Fit (GoF) test at the 1% significance level on the subband statistics for a three-scale DT-CWT. The null-hypothesis of the Chi-Square GoF test is that the data originates from a GGD. Regarding the filter parameterization of the DT-CWT, we use near-orthogonal (13,19)-tap filters on level one and Kingsbury's Q-shift (14,14)-tap filters [11] on levels ≥ 2. Table 1 summarizes the outcomes of the Chi-Square test for our six test images. A 0 signifies that the null-hypothesis could not be rejected at the given significance level for all images, while a number > 0 signifies the corresponding number of rejections. The first number gives the outcome for the real part, the second number gives the outcome for the imaginary part. As we can see, the null-hypothesis cannot be rejected for many of the tests at decomposition levels ≥ 2. Considering the fact that in case we assume a Normal distribution all null-hypothesis are rejected without exception, the GGD seems to be a quite good model here.

We further suggest that the real and imaginary parts of the coefficients of a given subband are realizations of i.i.d. random variables following one GGD with parameters α and β. Given that this assumption is actually valid, we can concatenate the real and imaginary parts to form a row vector $\mathbf{v}_{sk} = [\mathcal{R}(\mathbf{d}_{sk})\ \mathcal{I}(\mathbf{d}_{sk})]$ of dimensionality $2n_s^2$. Here, $\mathcal{R}(\cdot)$ denotes the real parts and $\mathcal{I}(\cdot)$ denotes the imaginary parts. To verify if the assumption holds, we conduct a number of two-sample Kolmogorow-Smirnow (KS) tests at the 1% significance level on the corresponding subband statistics. The null-hypothesis for the test is that both parts are drawn from the same underlying population. Table 2 lists the corresponding outcomes. Again a 0 denotes that the null-hypothesis cannot be rejected, numbers > 0 denote the number of rejections for our six test images. We observe that for levels ≥ 2 our assumption can not be rejected for the majority of cases. Thus, concatenation is reasonable and we can estimate the GGD parameters from $\mathbf{v}_{sk}$. For readability, we set $\mathbf{x} = \mathbf{v}^{sk}$. Further, let $N = 2n_s^2$ denote the dimensionality of $\mathbf{x}$. We use Maximum-Likelihood Estimation (MLE) to determine the GGD parameters throughout this work. The ML estimate for β is given as the solution to the transcendental, non-linear equation

$$\begin{aligned} 0 = 1 + \frac{\psi(1/\hat{\beta})}{\hat{\beta}} - \frac{\sum_{i=1}^{N} |x_i|^{\hat{\beta}} \log |x_i|}{\sum_{i=1}^{N} |x_i|^{\hat{\beta}}} + \\ \frac{\log\left(\frac{\hat{\beta}}{N}\sum_{i=1}^{N} |x_i|^{\hat{\beta}}\right)}{\hat{\beta}}. \end{aligned} \tag{2}$$

The parameter estimate $\hat{\beta}$ is then used to compute the MLE of the second parameter α as follows

$$\hat{\alpha} = \left(\frac{\hat{\beta}}{L}\sum_{i=1}^{L} |x_i|^{\hat{\beta}}\right)^{1/\hat{\beta}}. \tag{3}$$

To find the root of Eq. (2) we will resort to the classic Newton-Raphson root-finding iteration, which was proposed in [12] for example. An alternative would be to use moment estimate methods [10].

3. COMPLEX WAVELET TRANSFORM WATERMARKING

Generally speaking, additive spread-spectrum watermarking in the DT-CWT domain adds a pseudo-random watermark $\mathbf{w}$ to the host signal $\mathbf{x}$ to compute the watermarked signal $\mathbf{y}$ as $\mathbf{y} = \mathbf{x} + \mathbf{g} \cdot \mathbf{w}$, where the mask $\mathbf{g}$ is used to perceptually shape the watermark (Note: $\mathbf{g} \cdot \mathbf{w}$ denotes a point-wise multiplication). Since the CWT coefficients closely relate to human perception, a simple perceptual model can be used [13], where the elements of the mask $\mathbf{g}$ for subband $\mathbf{D}_{sk}$ are computed by

$$\mathbf{g}_{sk} = \sqrt{r^2 \cdot \overline{|\mathbf{d}_{sk}|_U^2} + \gamma^2}. \tag{4}$$

Here, $\overline{|\mathbf{d}_{sk}|_U^2}$ represents the averaged squared magnitude of neighboring CWT coefficients and $r \in \mathbb{R}$ and $\gamma \in \mathbb{R}$ are parameters depending on the decomposition level as well as orientation of the embedding subband (see [1]). The advantage of the DT-CWT over the DWT with biorthogonal 7/9 filters can be seen in the difference images of Figure 2. Due to the better directional selectivity of the DT-CWT, the embedded watermark better aligns with the texture of the image (especially visible in the lower-right area of Barbara's trousers). For a quantitative comparison see the results in section 5.1.

We note that the components of the random watermark $\mathbf{W}$ which lie in the null-space of the inverse transform of the redundant DT-CWT domain will be lost. The problem of embedding a spread-spectrum watermark in the DT-CWT domain can be overcome by adding the DT-CWT transformed watermark $\mathbf{W}'$ to the detail subbands, rather then adding the bipolar pseudo-random watermark $\mathbf{W}$ directly [13]. The watermark vector $\mathbf{w}'_{sk}$ used to watermark the host signal vector $\mathbf{v}_{sk}$ is obtained by decomposing the bipolar watermark image $\mathbf{W}$ in the same way as to host signal and again rearranging the watermark subband $\mathbf{W}'_{sk}$ into a row vector. In this work, we only use a scalar scaling factor g_{sk} per subband rather than a perceptual mask $\mathbf{g}_{sk}$.

In the literature, complex wavelet domain watermarking has been employed because its shift-invariance allows to compensate geometrical attacks and because of the superior perceptual characteristics due to the better directional sensitivity of its subbands compared to the DWT [13]. Woo et al. [3] construct an embedding domain invariant to geometric desynchronization attacks by applying the DT-CWT on top of the FFT and a log-polar mapping. For video watermarking, Earl et al. [4] presents a spread-transform, quantization-based scheme operating on a series on frames, exploiting the shift invariance property of the DT-CWT to resist spatial jitter. Wang et al. [5] employ scene-segmentation together with

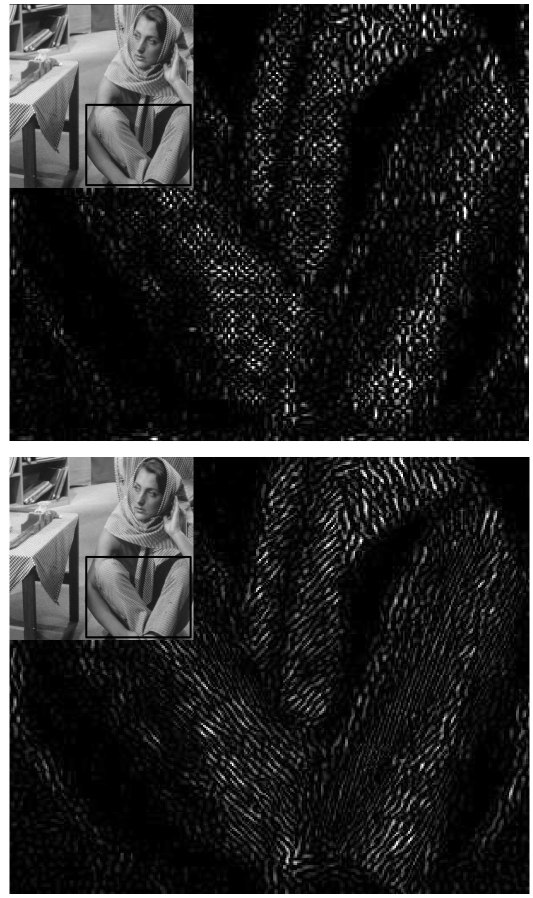

Fig. 2. Difference between original and watermarked images: DWT domain embedding (top) and DT-CWT domain embedding (bottom) at 40 dB PSNR

a 3D CWT for video watermarking. Coria et al. [6] embed a spread-spectrum watermark in the coarse subbands and correlate over multiple frames of a video sequence to achieve robustness against geometrical distortions. Two non-blind watermarking methods incorporate color images and describe combined visible/invisible watermarking [7, 8].

We now turn to blind watermark detection adapted to the DT-CWT domain host signal statistics. Previous work relies on linear correlation detection which is suboptimal for the non-Gaussian DT-CWT detail subbands.

4. BLIND DT-CWT WATERMARK DETECTION

In this section, we will first discuss the detection of the embedded watermark sequence using the classic GGD detector of [14] and the problems w.r.t. to our watermarking approach. Second, we introduce our proposed solution and discuss its advantages. For the following illustrations, we will omit the position indices s, k of the subbands in the DT-CWT decomposition structure and use $\mathbf{y}$ to denote a watermarked subband

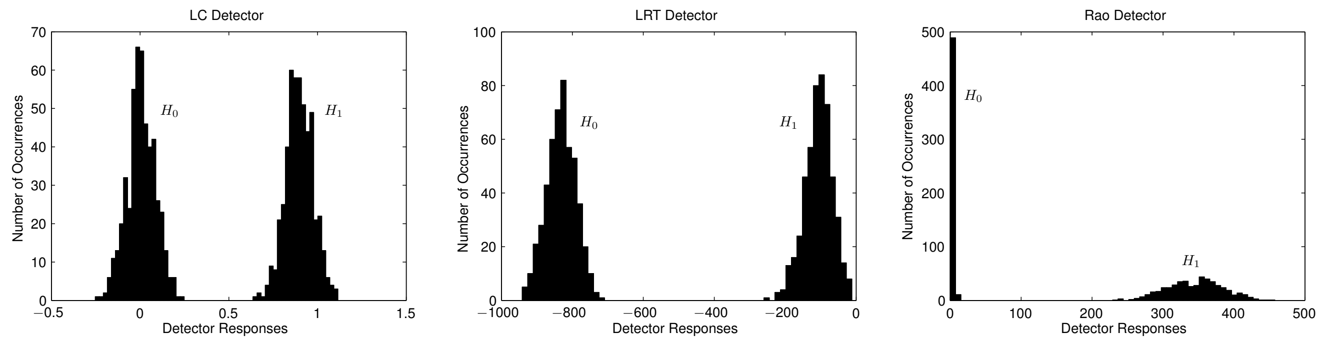

Fig. 3. Exemplary histograms of the LC, LRT and Rao detector responses under H_0 and H_1

vector with $N = 2n_s^2$ coefficients.

In [14], Hernandez et al. have derived a blind detector structure for host signals that can be modeled by a two-parameter GGD. Since the detector can be adapted to a given host signal via the GGD's shape parameter β, the detector demonstrates superior performance compared to a linear-correlation (LC) detector, which is optimal for a Gaussian host signal only. The log-likelihood ratio test (LRT) between the PDFs under H_0 (no watermark present) and H_1 (watermarked) of the GGD detector is given by

$$\rho_{LRT} = \sum_{i=1}^{N} \frac{1}{\alpha^\beta} \left(|y_i|^\beta - |y_i - gw_i|^\beta \right), \tag{5}$$

for a single scaling factor $g \in \mathbb{R}_+$. We note that the random elements in Eq. (5) are the coefficients of the watermark, not the y_i itself. Under the central limit theorem ($n \to \infty$), the log-likelihood ratio ρ_{LRT} (i.e. the detector response) follows a Gaussian distribution for which under H_0 the expectation value $\mathbb{E}[\rho_{LRT}|H_0] = \mu_{H_0}$ can be computed according to

$$\mu_{H_0} = \sum_{i=1}^{N} \frac{1}{\alpha^\beta} |y_i|^\beta - \frac{1}{2} \sum_{i=1}^{N} \frac{1}{\alpha^\beta} \left(|y_i - g|^\beta + |y_i + g|^\beta \right). \tag{6}$$

The variance $\mathbb{V}[\rho_{LRT}|H_0] = \sigma_{H_0}^2$ can be easily derived,

$$\sigma_{H_0}^2 = \frac{1}{4} \sum_{i=1}^{N} \frac{1}{\alpha^{2\beta}} \left(|y_i + g|^\beta - |y_i - g|^\beta \right)^2. \tag{7}$$

The expectation and variance under the alternative hypothesis H_1, denoted as $\mu_{H_1}, \sigma_{H_1}^2$, have been shown to be $\mu_{H_1} = -\mu_{H_0}$ and $\sigma_{H_1}^2 = \sigma_{H_0}^2$, respectively. According to the Neyman-Pearson criterion, we can select the detection threshold T based on a desired probability of false-alarm P_f as $T = \sigma_{H_0} \cdot \mathrm{Q}^{-1}(P_f) - \mu_{H_0}$ where $\mathrm{Q}(\cdot)$ denotes the Q-function to express right-tail probabilities of the Normal distribution. The probability of miss P_m is given by

$$P_m = \mathbb{P}(\rho_{LRT} < T|H_1) = 1 - Q\left(Q^{-1}(P_f) - 2\frac{\mu_{H_1}}{\sigma_{H_1}} \right). \tag{8}$$

However, there is one important restriction to be considered. Eqs. (6) and (7) only hold for watermarks following a discrete distribution with equiprobable values $\{-1, +1\}$. Our experimental results based on 1000 randomly generated watermarks with equiprobable values $\{+1, -1\}$ show that the transformed watermark $\mathbf{W}'$ follows a Gaussian distribution with zero mean and approximate variance of 0.25. Therefore, Eqs. (6) and (7) cannot be applied any longer. Since we do not have a closed form expression for Eqs. (6) and (7) for the normally distributed subband statistics of $\mathbf{W}'$, we have to resort to empirical estimates of μ_{H_0} and $\sigma_{H_0}^2$ for a given signal, in order to determine a reasonable detection threshold T. Unfortunately, this is a cumbersome procedure in practice.

We can find a solution to that problem in signal detection theory [15]. In particular, we adopt a Rao hypothesis test which has already been extensively discussed in a general signal detection setting by [16] and was proposed by [17] for the purpose of blind spread-spectrum watermark detection in the DWT domain. However, our setup is slightly different from the one presented in [17]. First, our watermark is not bipolar but Normal and second, we use another, but equivalent parametrization of the GGD (see Eq. (1)). Provided that $p(\cdot)$ denotes a symmetric PDF, the general formulation of the Rao hypothesis test derived in [16] is given by

$$\rho_{Rao} = \frac{\left[\sum_{i=1}^{N} \left. \frac{\partial \log p(y_i - gw_i, \gamma)}{\partial g} \right|_{g=0} \right]^2}{\frac{1}{N} \sum_{i=1}^{N} w_i^2 \left(\sum_{i=1}^{N} \left[\frac{p'(y_i,\gamma)}{p(y_i,\gamma)} \right]^2 \right)}, \tag{9}$$

where p' denotes the first derivative of the PDF w.r.t. y_i and $\gamma \in \mathbb{R}^d$ denotes an arbitrary d-dimensional parameter vector. In signal detection theory, the elements of γ are termed the *nuisance* parameters, which are unknown and have to be estimated. Inserting the PDF of the GGD ($\gamma = [\alpha\ \beta]$) now leads to our desired detection statistic

$$\rho_{Rao} = \frac{\left[\sum_{i=1}^{N} w_i \operatorname{sgn}(y_i) |y_i|^{\beta-1} \right]^2}{\frac{1}{N} \sum_{i=1}^{N} w_i^2 \left(\sum_{i=1}^{N} |y_i|^{2\beta-2} \right)}, \tag{10}$$

where $\operatorname{sgn}(\cdot)$ denotes the signum function. We note that in contrast to the Rao detector for bipolar watermarks, the sum over the squared watermark elements in the denominator of Eq. (10) cannot be dropped. From the theory of statistical signal detection we know that detection statistic under H_0 follows a Chi-Square distribution with one degree of freedom. Under the alternative hypothesis H_1, the detection statistic follows a Non-Central Chi-Square distribution with one degree of freedom and non-centrality parameter λ. We can determine the detection threshold T based on a desired P_f as $T = Q^{-1}(P_f/2)^2$. The probability of missing the watermark (P_m) is given by

$$P_m = \mathbb{P}(\rho_{Rao} < T|H_1) = \\ 1 - \mathrm{Q}(\mathrm{Q}^{-1}(P_f/2) - \sqrt{\lambda}) - \mathrm{Q}(\mathrm{Q}^{-1}(P_f/2) + \sqrt{\lambda}). \tag{11}$$

Alternatively, P_m can be computed using the CDF of the Non-Central Chi-Square distribution. To illustrate the difference in the detector output statistics, Figure 3 shows exemplary histograms of the detector responses (Lena) for the linear-correlation (LC) detector, the likelihood-ratio test (LRT) and the Rao detector. We note that the responses of the first two detectors follow Normal distributions with approximately equal variances under H_0 and H_1 while the detection responses of the Rao test can be modeled by the aforementioned Chi-Square distributions.

5. EXPERIMENTAL RESULTS

In this section, we present the experimental results of our work.[1] Our six 256×256 grayscale test images are shown in Figure 4. We begin by justifying the more involved DT-CWT domain embedding over the use of the DWT domain and then report detection performance results.

5.1. Perceptual Assessment

We have already observed the superior perceptual characteristics of DT-CWT embedding in Figure 2, Section 3. For an objective assessment of the distortion caused by DT-CWT and DWT embedding with the same PSNR, we employ four perceptual metrics, wPSNR/PQS [18], Komparator[2] [19], C4 [20] and VSNR[3] [21] which all have been proposed to assess compression artifacts without making assumptions about the type of degradation introduced by coding schemes. Komparator and C4 have already been successfully applied to the perceptual assessment of watermarking schemes [22]. In Table 4 we present the perceptual quality measures for DWT and DT-CWT embedding according to our chosen metrics. The embedding strength has been adjusted to obtain watermarked images of 36 dB PSNR, so that the watermark becomes slightly noticeable in smooth and edge regions. DT-CWT embedding results in better image quality with the exception of the texture image Fabric which lacks any diagonal features. Note that for Komparator, lower values correspond to better perceptual quality, and vice-versa for wPSNR/PQS, C4 and VSNR .

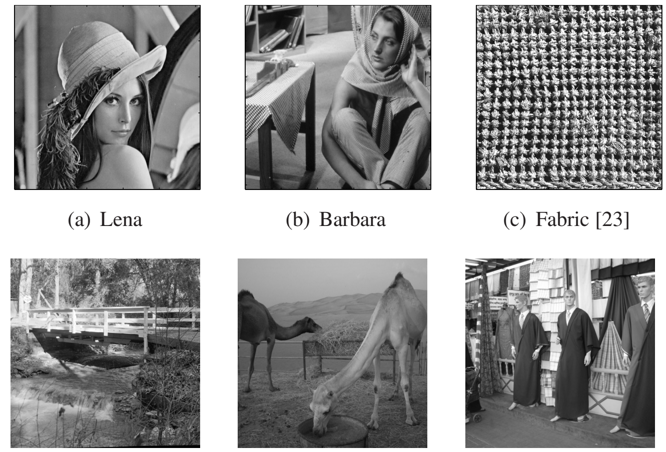

(a) Lena (b) Barbara (c) Fabric [23]

(d) Bridge (e) Dromedary (f) Models

Fig. 4. Example images

Image	PSNR	Image	PSNR
Barbara	48.21	Bridge	46.73
Dromedary	52.42	Fabric	38.60
Lena	47.16	Models	44.55

Table 3. Average PSNR (dB) for our watermarked images (embedding with 16 dB DWR)

In addition to our selected example images, the objective quality assessment has also been performed on 500 other natural grayscale images of size 512×512 (taken from the BOWS-2 image set[4]). Komparator claimed superior quality for the DT-CWT embedding in 382 cases versus 118 for DWT, while C4 votes 422 times for DT-CWT and 78 times for DWT. wPSNR/PQS and VSNR decided in all cases in favour of the DT-CWT embedding approach. To our knowledge, this is the first objective quality assessment comparing two watermark embedding domains – further study is needed.

5.2. Detection Results

For a comparison of the detection performance, we arbitrary choose to embed the watermark sequence at decomposition level two (subband $+45°$). The resulting PSNRs for the watermarked images (16 dB Document-to-Watermark Ratio, DWR) are shown in Table 3.

First, we analyze the performance of our detectors in the absence of attacks, see Figure 5. We determine the experi-

[1]Our MATLAB source will be available online at `http://www.wavelab.at/sources`.

[2]Komparator source code is available at `http://autrusseau.florent.club.fr/Komparator`.

[3]VSNR source code is available at `http://foulard.ece.cornell.edu/dmc27/vsnr/vsnr.html`.

[4]BOWS-2 is online at `http://bows2.gipsa-lab.inpg.fr/`.

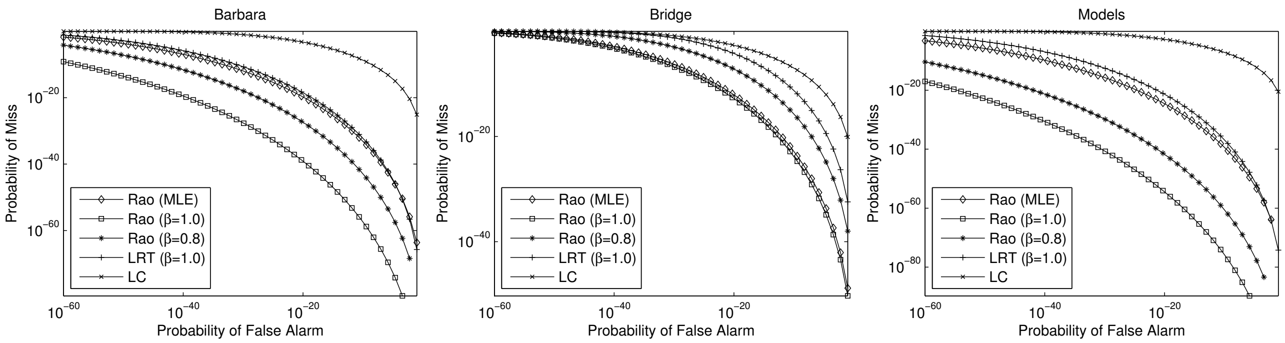

Fig. 5. Detector ROC plots for 16 dB DWR

Image	wPSNR/PQS [18]		Komparator [19]		C4 [20]		VSNR [21]	
	DWT	DT-CWT	DWT	DT-CWT	DWT	DT-CWT	DWT	DT-CWT
Lena	45.88	**46.49**	992.28	**799.57**	0.939	**0.950**	23.48	**26.53**
Barbara	46.81	**47.26**	1045.24	**400.61**	0.954	**0.957**	24.63	**27.78**
Fabric	46.19	**46.90**	**198.86**	320.72	**0.966**	0.965	30.88	**34.67**
Bridge	45.96	**46.49**	556.719	**506.745**	0.941	**0.960**	26.21	**29.43**
Dromedary	45.95	**46.52**	1059.48	**387.69**	0.923	**0.946**	22.78	**25.56**
Models	45.75	**46.29**	672.59	**444.81**	0.957	**0.963**	28.60	**31.90**

Table 4. wPSNR/PQS, Komparator, C4 and VSNR quality metric for DWT and DT-CWT embedding with 36 dB PSNR

mental ROC curves from test runs with 1000 randomly generated watermarks (simulating the H_1 hypothesis). Only in case of the LRT detector, we have to resort to estimating the mean and variance of the normally distributed detection statistic under H_0 as well. We have further verified that the detector responses of the Rao detector under H_0 actually follow a Chi-Square distribution with one degree of freedom using a GoF test at 1% significance.

To compute the ROC curves of the Rao detector we estimate the non-centrality parameter λ from the ρ_{Rao} as follows: since we know that under H_1 the square-root of the detection statistic will follow a Normal distribution $\mathcal{N}(\sqrt{\lambda}, 1)$, we can simply estimate λ by raising the arithmetic mean of $\sqrt{\rho_{Rao}}$ to the power of two. Then, we can determine P_m at a given P_f from the Eq. (11). As expected, the LC detector employed by previous DT-CWT domain watermarking schemes [13, 4, 3, 5, 6] performs worst. Interestingly, using the MLE of the shape parameter β did not result in the best detection performance for the Rao and LRT detector. To find a reasonable explanation for this behavior, we have to take a closer look at the embedding process. What we actually do, is to add a scaled random sequence (the watermark), which follows a Gaussian law, to the transform coefficients following a Generalized Gaussian law. Depending on the embedding strength, this has the effect that the shape parameter β is altered. Due to the redundancy of the DT-CWT, the marked coefficients will be partly lost during the inverse transform. This leads to the situation that at the detection stage, β cannot be accurately estimated any longer, which in turn leads to poor detection performance. However, our experiments show that for reasonable DWRs, a fixed shape parameter $\beta = 1$ performs very well, since after embedding the GGD shape is close to one for natural images. Therefore, we will perform the detection performance analysis under attacks with this fixed shape parameter $\beta = 1$. The ROC results for the other test images are similar but we omit them due to space limitations.

We consider JPEG and JPEG 2000 compression with varying quality factors and bit rates to evaluate the detectors' performance under attack in Figures 6 and 7. For the JPEG attacks we use MATLAB's functionality to write JPEG images with quality factors ranging from 10 to 90. In case of JPEG2000, we employ the Kakadu toolkit[5] with bit rates ranging from 0.2 bpp to 1.4 bpp. The LC detector shows the worst performance. Concerning the LRT and Rao detector, Rao is consistently better than LRT for both attacks at the P_f of 10^{-10}. Setting the GGD's shape parameter $\beta = 1$ only limits the detection performance for the texture image Fabric, where the true shape of the GGD significantly differs from $\beta = 1$ and is close to two.

6. CONCLUSION

The contribution of this paper is threefold: First, we show that the concatenated marginal statistics of the real and imaginary coefficient components of the DT-CWT detail subbands can be modeled by GGDs. Since the shape parameters of

[5]Kakadu binaries are available at `http://kakadusoftware.com`.

fitted GGDs differ significantly from the Gaussian distribution in case of natural images, the blind linear correlation detection employed by earlier DT-CWT watermarking schemes [13, 4, 3, 5, 6] can be improved. To this end, we have adapted the GGD detector structure proposed by [14] to work with the DT-CWT and discussed the problem of threshold determination. Further, we have proposed a modification of the Rao detector presented in [17] to work with our watermarking setup in order to overcome the problems related to the LRT detector. Second, our experimental results indicate that an estimation of the shape parameter of the GGD leads to poorer detection performance than setting β to a fixed value. The explanation of this behavior is strongly related to the redundancy of the DT-CWT and the distributional properties of the transformed watermark. Last, detection results under JPEG and JPEG2000 attacks highlight the advantages of the Rao detector and justify our approach. Further work will include a detailed examination of the parameter estimation issues, investigate the impact of perceptual modelling and continue the perceptual assessment of the watermarked images.

REFERENCES

[1] P. Loo and N. Kingsbury, "Digital watermarking using complex wavelets," in *Proceedings of the IEEE International Conference on Image Processing, ICIP '00*, Vancouver, Canada, Sept. 2000, vol. 3, pp. 29–32.

[2] N. Kingsbury, "The Dual-Tree Complex Wavelet Transform: A new Technique for Shift-Invariance and Directional Filters," in *Proceedings of the 8th IEEE DSP Workshop*, Bryce Canyon, UT, USA, Aug. 1998, pp. 9–12.

[3] Ch. Woo, J. Du, and B. Pham, "Geometric invariant domain for image watermarking," in *Proceedings of the International Workshop on Digital Watermarking, IWDW '06*, South Korea, Nov. 2006, vol. 4283 of *Lecture Notes in Computer Science*, pp. 294–307, Springer.

[4] J. Earl and N. Kingsbury, "Spread transform watermarking for video sources," in *Proceedings of the IEEE International Conference on Image Processing, ICIP '03*, Barcelona, Spain, Sept. 2003, vol. 2, pp. 491–494.

[5] J. Wang, X. Gao, and J. Zhong, "A video watermarking based on 3-D complex wavelet," in *Proceedings of the IEEE International Conference on Image Processing, ICIP '07*, San Antonio, TX, USA, Sept. 2007, vol. V, pp. 493–496, IEEE.

[6] L. Coria, M. Pickering, P. Nasiopoulos, and R. Ward, "A video watermarking scheme based on the dual-tree complex wavelet transform," *IEEE Transactions on Information Forensics and Security*, vol. 3, no. 3, pp. 466–474, Sept. 2008.

[7] S. Mabtoul, E. Hassan, I. Elhaj, and D. Aboutajdine, "Robust color image watermarking based on singular value decomposition and dual tree complex wavelet transform," in *Proceedings of the 14th IEEE International Conference on Electronics, Circuits and Systems, ICECS '07*. Dec. 2007, pp. 534–537, IEEE.

[8] L. Zhuang and M. Jiang, "Multipurpose digital watermarking algorithm based on dual-tree CWT," in *Proceedings of the 6th International Conference on Intelligent Systems, Design and Applications, ISDA '06*, Oct. 2006, vol. 2, pp. 316–320.

[9] H. Malvar and D. Florencio, "Improved spread spectrum: A new modulation technique for robust watermarking," *IEEE Transactions on Signal Processing*, vol. 51, no. 4, pp. 898–905, Apr. 2003.

[10] S. Nadarajah, "A generalized normal distribution," *Journal of Applied Statistics*, vol. 32, no. 7, pp. 685–694, Sept. 2005.

[11] N. Kingsbury, "Complex Wavelets for Shift-Invariant Analysis and Filtering of Signals," *Journal of Applied Computational Harmonic Analysis*, vol. 10, no. 3, pp. 234–253, 2001.

[12] M. Do and M. Vetterli, "Texture Similarity Measurement using Kullback-Leibler Distance on Wavelet Subbands," in *Proceedings of the IEEE International Conference on Image Processing, ICIP '00*, Vancouver, Canada, Sept. 2000, vol. 3, pp. 703–733.

[13] P. Loo, *Digital Watermarking with Complex Wavelets*, Ph.D. thesis, University of Cambridge, United Kingdom, Mar. 2002.

[14] J. Hernández, M. Amado, and F. Pérez-González, "DCT-domain watermarking techniques for still images: Detector performance analysis and a new structure," *IEEE Transactions on Image Processing*, vol. 9, no. 1, pp. 55–68, Jan. 2000.

[15] S. Kay, *Fundamentals of Statistical Signal Processing: Detection Theory*, vol. 2, Prentice-Hall, 1998.

[16] S. Kay, "Asymptotically optimal detection in incompletely characterized non-gaussian noise," *IEEE Transactions on Acoustics, Speech and Signal Processing*, vol. 37, no. 5, pp. 627–633, May 1989.

[17] A. Nikolaidis and I. Pitas, "Asymptotically optimal detection for additive watermarking in the DCT and DWT domains," *IEEE Transactions on Image Processing*, vol. 12, no. 5, pp. 563–571, May 2003.

[18] M. Miyahara, "Objective picture quality scale (PQS) for image coding," *IEEE Transactions on Communications*, vol. 46, no. 9, pp. 1215–1226, Sept. 1998.

[19] D. Barba and P. Le Callet, "A robust quality metric for color image quality assessment," in *Proceedings of the IEEE International Conference on Image Processing, ICIP '03*, Barcelona, Spain, Sept. 2003, vol. 1, pp. 437–440, IEEE.

[20] M. Carnec, P. Le Callet, and D. Barba, "Objective quality assessment of color images based on a generic perceptual reduced reference," *Signal Processing: Image Communication*, vol. 23, no. 4, pp. 239–256, Apr. 2008.

[21] D. Chandler and S. Hemami, "VSNR: A wavelet-based visual signal-to-noise ratio for natural images," *IEEE Transactions on Image Processing*, vol. 16, no. 9, pp. 2284–2298, Sept. 2007.

[22] E. Marini, F. Autrusseau, P. Le Callet, and P. Campisi, "Evaluation of standard watermarking techniques," in *Proceedings of SPIE, Security, Steganography and Watermarking of Multimedia Contents IX*, San Jose, CA, USA, Jan. 2007, vol. 6505.

[23] "MIT vision and modeling group," [Online], Available: http://vismod.media.mit.edu.

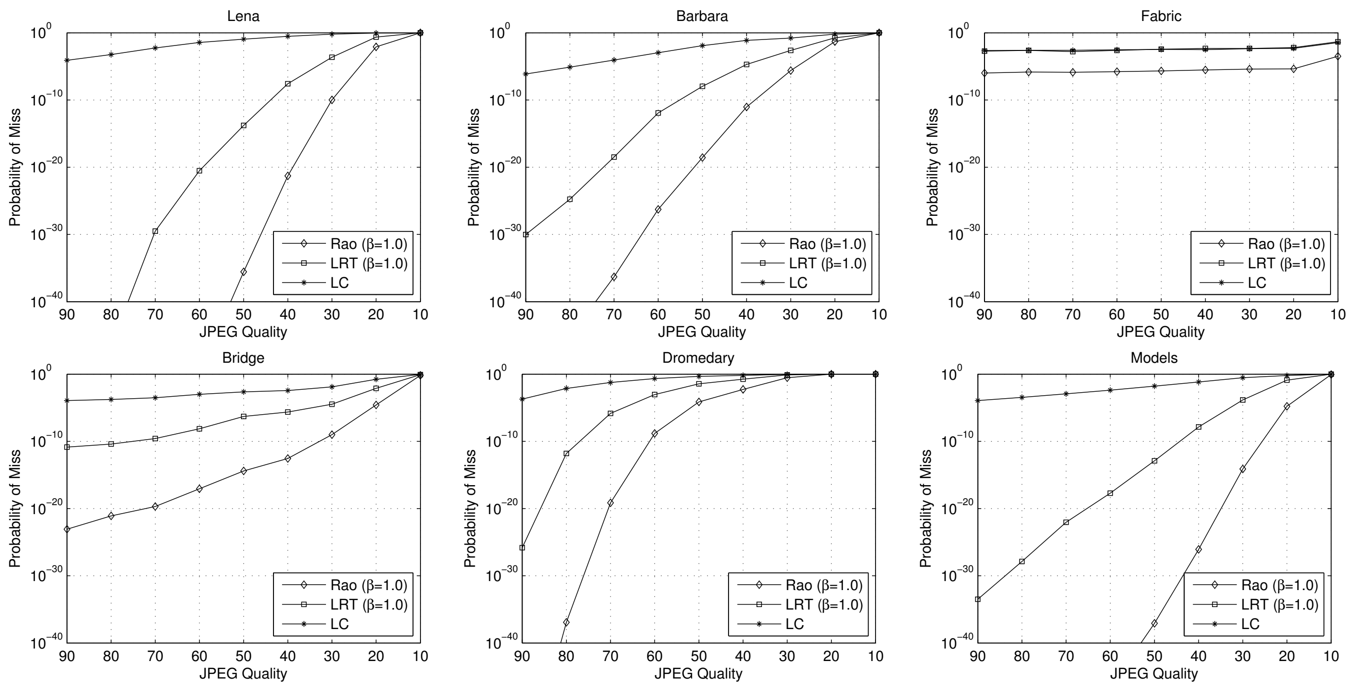

Fig. 6. JPEG attack results for $P_f = 10^{-10}$ and DWR 16 dB

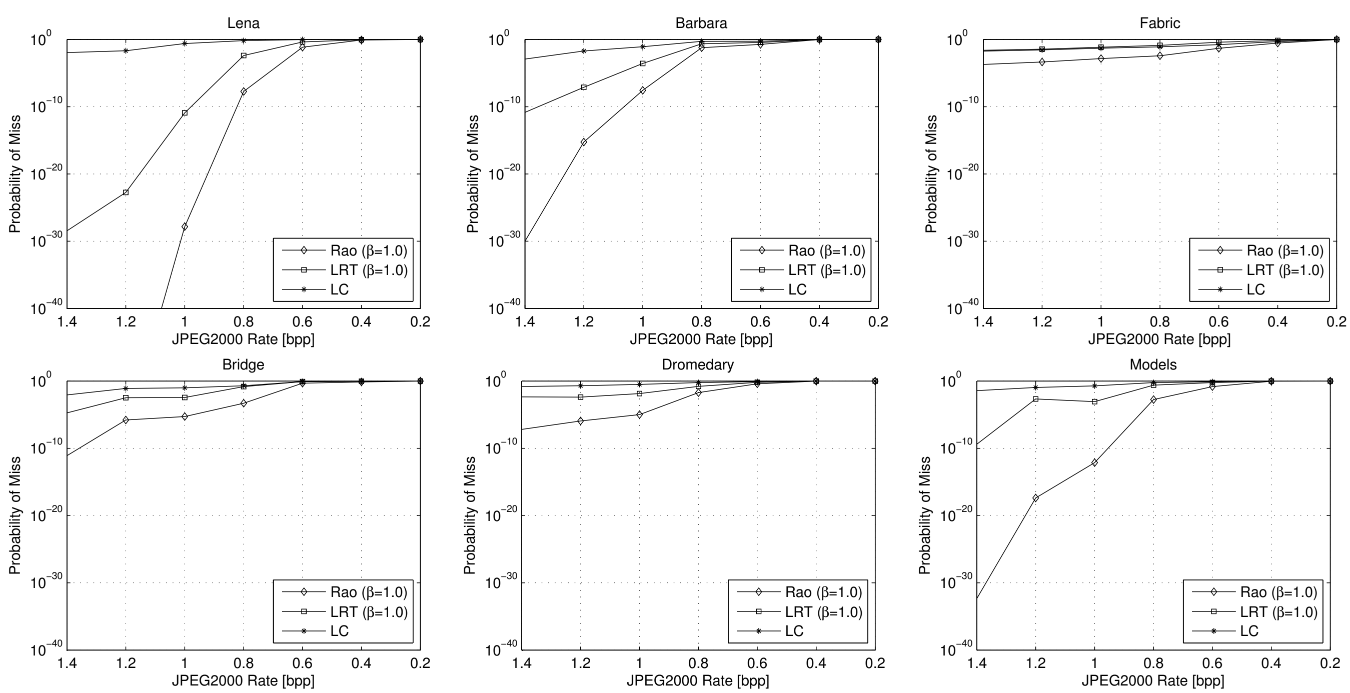

Fig. 7. JPEG2000 attack results for $P_f = 10^{-10}$ and DWR 16 dB